Journal of Magnetics 7(3), 72-79 (2002)

Local Variation of Magnetic Parameters of the Free Layer in TMR Junctions

CheolGi Kim*, Toshihiro Shoyama[1], Masakiyo Tsunoda[1], Migaku Takahashi[1], Tae Hyo Lee and Chong-Oh Kim

Department of Materials Engineering, Chungnam National University, Taejon 305-764, Korea
[1]Department of Electronic Engineering, Tohoku University, Sendai 980-8579, Japan

(Received 2 August 2002)

Local M-H loops have been measured on the free layer of a tunneling magnetoresistance (TMR) junction using the magneto-optical Kerr effect (MOKE) system, with an optical beam size of about 2 μm diameter. Tunnel junctions were deposited using the DC magnetron sputtering method in a chamber with a base pressure of 3 $\times 10^{-9}$ Torr. The relatively irregular variations of coercive force H_c (~17.5 Oe) and unidirectional anisotropy field H_{ua} (~7.5 Oe) in the as-deposited sample are revealed. After 200 °C annealing, H_c decreases to 15 Oe but H_{ua} increases to 20 Oe with smooth local variations. Two-dimensional plots of H_c and H_{ua} show the symmetric saddle shapes with their axes aligned with the pinned layer, irrespective of the annealing field angle. This is thought to be caused by geometric effects during deposition, together with a minor annealing effect. In addition, the variation of root mean square (RMS) surface roughness reveals it to be symmetric with respect to the center of the pinned-layer axis, with the roughness of 2.5 Å near the edge and 5.8 Å at the junction center. Comparison of surface roughness with the variation of H_{ua} suggests that the H_{ua} variation of the free layer is well described by dipole interactions related to surface roughness. As a whole, the reversal magnetization is not uniform over the entire junction area and the macroscopic properties are governed by the average sum of local distributions.

Key words : Coercivity, Exchange coupling, MOKE, Surface roughness, TMR

1. Introduction

Magnetic tunnel junctions (MTJs) consisting of two ferromagnetic layers separated by a thin insulating layer (typically Al_2O_3) show large tunneling magnetoresistance (TMR), which makes them promising candidates for magnetic random access memory (MRAM) devices [1, 2]. As is generally known [3, 4], the tunneling resistance will be large in a field regime, with antiparallel magnetizations of the two layers. For all other field regimes, the magnetizations in both electrodes are parallel and the resistance will have a lower value. Thus, resistance characteristics are governed by the ferromagnetic-antiferromagnetic states of the two magnetic layers during cyclic magnetization. Most researchers have dealt with the materials and fabrication parameters controlling the coercive forces and exchange coupling caused by interlayer coupling [5, 6], rather than examining the way in which magnetization reversal governs magnetoresistance (MR) characteristics.

The magnetization reversal in a stack of thin films may be strongly affected by various magnetic parameters. One important parameter is unidirectional anisotropy (the exchange coupling) caused by the interlayer coupling between adjacent films. The main interlayer coupling effects have been identified to be RKKY-like coupling through an indirect exchange mediated by the itinerant electrons, and Neel's orange peel coupling from magnetic dipole interaction related to interfacial morphological corrugations [7-9]. When an insulating layer prevents electron itinerancy, dipole interaction is reasonable, rather than RKKY-like coupling.

The dipole interaction is a function of the correction length, the height of the sinusoidal roughness of the interface surface, and the thickness of each magnetic layer [10]. Even though interface roughness of NiFe/MnIr, measured by the XRD method, is not equal to surface roughness measured by the atomic force microscope, there is quantitative agreement between them [11]. However, there are contradictory results for the correlation between exchange coupling and surface roughness; while

*Corresponding author: Tel: +82-42-821-6229
e-mail: cgkim@cnu.ac.kr

one result indicates that the exchange coupling is inversely proportional to surface roughness [11, 12], another result claims that the exchange coupling is proportional to surface roughness [13]. A full understanding of their relationship has not been attained, because of the complicated material and magnetic parameters.

In reality, because of the inhomogeneity of material parameters, magnetization in both magnetic layers can be nonuniform over the sample with a corresponding distribution of reversals. This distribution probably arises from local variations in magnetic anisotropy and/or coupling from grain to grain within each layer. The magnetization reversal distribution could play a decisive role in the MR ratio and its field sensitivity. However, very few papers have reported MR dependence on exchange coupling strength between two magnetic layers, and the intrinsic pinning field governing magnetization reversal [14, 15]. In this work, we have measured the local distributions of coercive forces, as well as uniaxial anisotropy and surface roughness on MTJs prepared using DC sputtering. We discuss the measured magnetic parameters as functions of surface roughness and the annealing field angle.

2. Experimental Procedure

Tunnel junctions with the structure of Ta (50 Å)/Cu (100 Å)/Ta (50 Å)/Ni-Fe (20 Å)/Cu (50 Å)/$Mn_{75}Ir_{25}$ (100 Å)/$Co_{70}Fe_{30}$ (25 Å)/Al-O/$Co_{70}Fe_{30}$ (25 Å) were prepared on thermally oxidized Si wafers using DC magnetron sputtering in a chamber with a base pressure of 3×10^{-9} Torr. For barrier formation, a 15-Å-thick metallic Al film was deposited and subsequently oxidized in an oxidation chamber with a radial line slot antenna (RLSA) for 2.45-GHz microwaves [16]. Kr was used as the inert gas mixed with O_2 molecular gas for the plasma oxidation. In-situ patterned junctions were prepared using a shadow mask during deposition. The junction size was 180×180 μm^2.

The junction samples were thermally annealed at 200 °C for 1 hour under a magnetic field of 1 kOe, followed by field cooling. The angle θ_a between the annealing field and the pinned-layer axis varied from 0° to 90°. The transport measurement was performed with a four-point probe method at room temperature for samples with electrode layers of 1000-Å NiFe, deposited on the free layer Co-Fe. In these samples, the maximum TMR ratio was measured to be 40% in a 270 °C field-annealed sample.

The magneto-optical Kerr effect (MOKE) method was used to obtain the local M-H loops under a 50 Hz driving field, as depicted in Fig. 1. The penetration depth using He-Ne laser light was about 30 nm, which was enough to

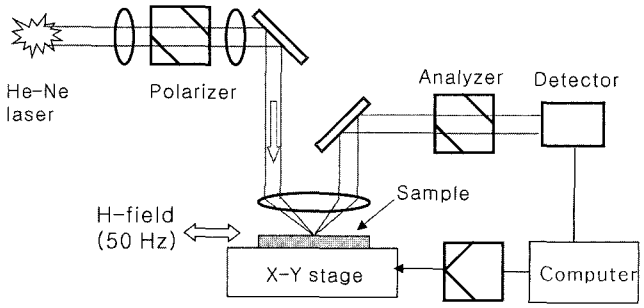

Fig. 1. Schematic view of micro-MOKE (magneto-optical Kerr effect) system.

affect the whole thickness of the free layer. The field was applied in the annealing field direction. The maximum field amplitude was 100 Oe, which was enough to saturate the free layer in the multilayer structure. The laser beam size was about 2 μm diameter, corresponding to the spatial resolution of the micro-MOKE system. The sample was scanned using a computer-controlled x-y stage to obtain a two-dimensional plot of magnetic parameters. Surface roughness was measured by atomic force microscopy (AFM) at different points across the junction.

3. Results and Discussion

3.1. Local variation

Figures 2(a)~(f) show the measured M-H loops at several positions along the free-layer direction (y-axis), as depicted in the inset. Here, the sample was annealed once at a temperature of $T_a = 200$ °C and the annealing field angle $\theta_a = 0°$. The M-H loop was measured under a cyclic field along the pinned-layer direction, that is, the annealing field direction. There is no shift of loop at the outside edge of the junction, as shown in Fig. 2(a). The

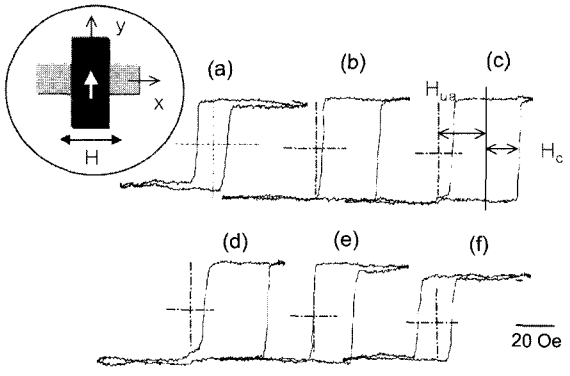

Fig. 2. M-H loops along the free-layer direction (y-axis), at the positions (a) 0, (b) 105, (c) 130, (d) 165, (e) 205, and (e) 285 μm. The starting point is 50 μm below the junction edge.

shift due to the unidirectional anisotropy (bias) field H_{ua} increases as the measuring point moves to the junction center, as shown in Figs. 2(b) and (c), but then decreases as the point moves away from the center. We can also see similar variation of the coercive force H_c . Even though there are local variations of both H_c and H_{ua}, the squareness ratio of the loops is nearly equal to one, except for the loops caused by demagnetizing effects when the measuring point is less than about 10 μm distant from the edge boundary.

Two-dimensional plots of maximum amplitude of Kerr signal, obtained using a 20×20 scan, are shown in Figs. 3(a), (b) for as-deposited and 200 °C-annealed samples, respectively. The signal of MOKE could be affected by the experimental parameters of extinction ratio of polarizer, optical reflectivity and analysizer angle, and by material parameter of Kerr rotation. Because the experimental parameters are fixed during the measurement, maximum Kerr signal corresponds with the maximum magnetization of free layer. There is an irregular variation of maximum Kerr signal in the as-deposited sample even near the center of the free layer. There is also a gradual increase from edge, and it reaches 90% of the center value at 30 μm distance from the boundary. This variation is caused by the gradual change of film thickness arising from edge effects during deposition using a mask. The thickness variation was checked by the α-stepper as shown in the inset figure. After annealing, the irregular variation becomes smooth out over the junction area except in the edge region.

The variations of H_c and H_{ua} for an annealed sample are compared with those for an as-deposited one in Figs. 4(a) and (b), respectively. The H_c in the as-deposited sample is about 10 Oe outside the junction, and a maximum of 17.5 Oe at the junction center. The local variation is quite irregular, with changes of 5 Oe, as shown in Fig. 4(a). As a whole, H_c is reduced after field annealing, while the local variation becomes smooth and reveals symmetry with respect to the center of the pinned-layer axis. H_c decreases with annealing temperature up to 250 °C, and then is nearly constant.

In Fig. 4(b), H_{ua} is induced during the sample deposition, with a maximum of 7.5 Oe at the junction center in

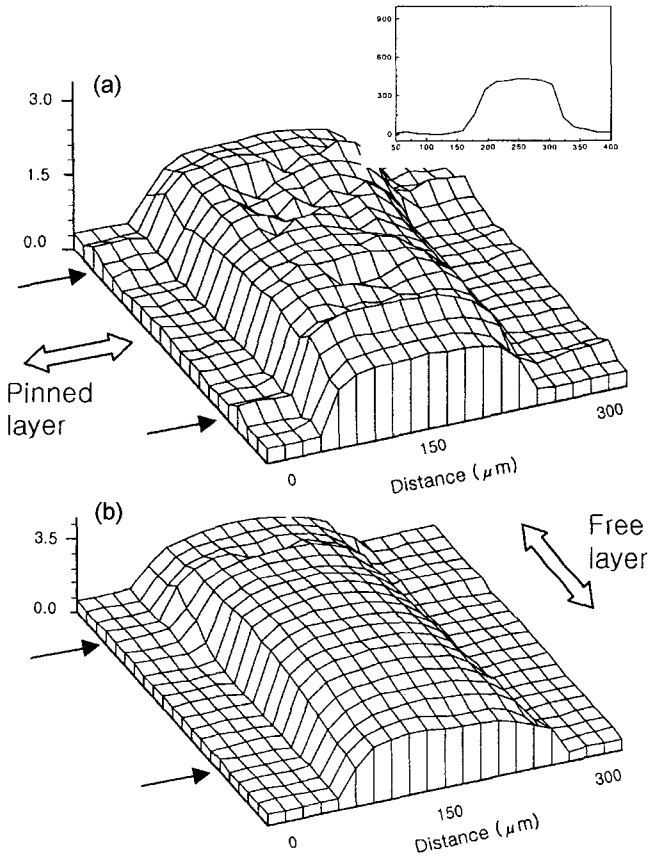

Fig. 3. Two-dimensional distribution of maximum magnetization (a) as-deposited (b) 200 °C-annealed sample for the annealing field angle $\theta_a = 0°$. (Inset figure: variation of film thickness across the junction center, checked by α-stepper.)

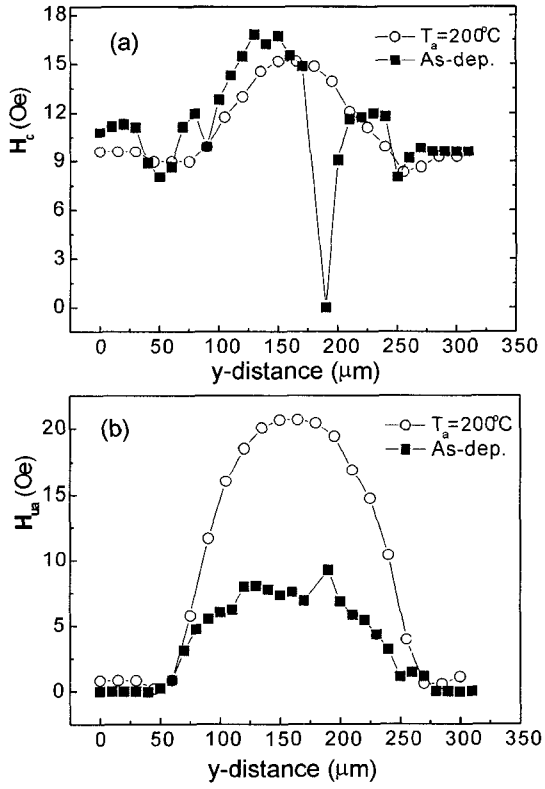

Fig. 4. Variation of (a) coercive force H_c and (b) unidirectional bias field H_{ua} along the free-layer axis in as-deposited and 200 °C-annealed samples.

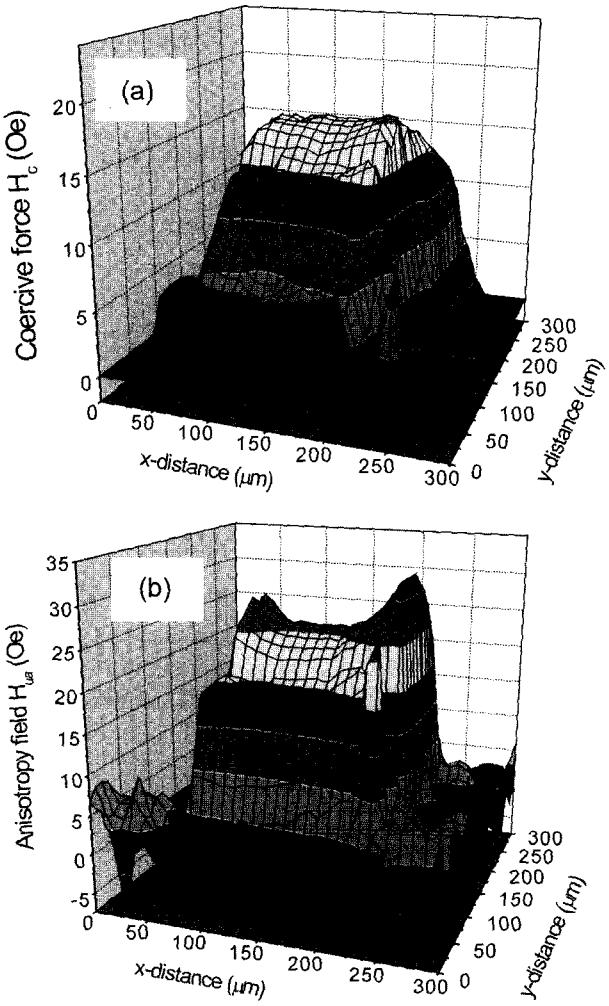

Fig. 5. Two-dimensional distribution of (a) coercive force H_c, and (b) unidirectional anisotropy field H_{ua} in 200 °C-annealed sample for the annealing field angle $\theta_a = 0°$. (x-axis: pinned layer, y-axis: free-layer directions)

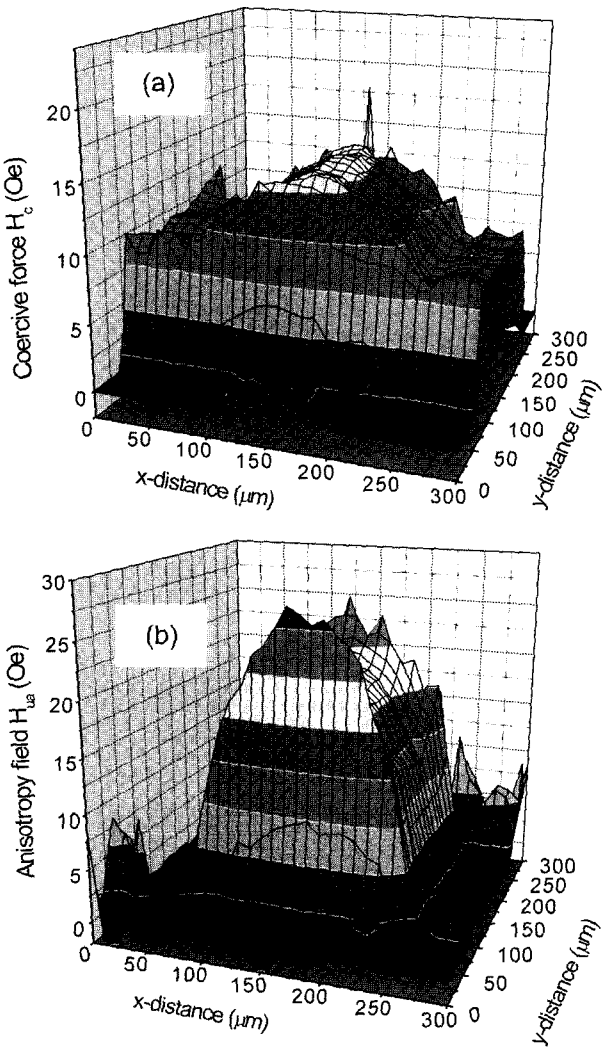

Fig. 6. Two-dimensional distribution of coercive force H_c and unidirectional anisotropy field H_{ua} in 200 °C-annealed sample for the annealing field angle $\theta_a = 90°$. (x-axis: free layer, y-axis: pinned layer directions)

the as-deposited sample and irregular variation. However, the field annealing enhances the H_{ua} up to 20.5 Oe at the center. Similarly to H_c, H_{ua} shows smooth variation along the free layer; that is, the zero-value of H_{ua} gradually increases to 25 Oe at the junction center. As we describe later, magnetic dipole interaction between the free and pinned layers is an origin of H_{ua}. Thus, the above-described changes of H_{ua} might be influenced by the changes of the exchange anisotropy of *pinned layer* during field annealing. The bias field of the antiferromagnetic layer is known to be a function of the MnIr thickness and the annealing temperature [17]. For 100-Å MnIr thickness, the exchange anisotropy gradually increases with increasing annealing temperature up to $T_a = 400$ °C.

Figures 5(a) and (b) are two-dimensional plots of H_c and H_{ua}, respectively, on the annealed sample for $T_a = 200$ °C, where measuring points are scanned over the entire junction area. Both H_c and H_{ua} show a saddle shape with its axis along the pinned-layer axis, where local variations along the pinned-layer axis are relatively small, compared to those in the free-layer direction. As a whole, local variations of H_c and H_{ua} over the junction area are significant compared to the maximum magnetization.

When the sample is annealed under a magnetic field in the free-layer axis, that is, $\theta = 90°$, the M-H loops measured on the free- and pinned-layer axes clearly reveal the change of the magnetically easy axis according to the annealing field. Figure 6 shows the two-dimensional distribution of H_c and H_{ua}, where the loops are measured under the field in the free-layer axis. The local distributions of H_c and H_{ua} also show saddle shapes with their

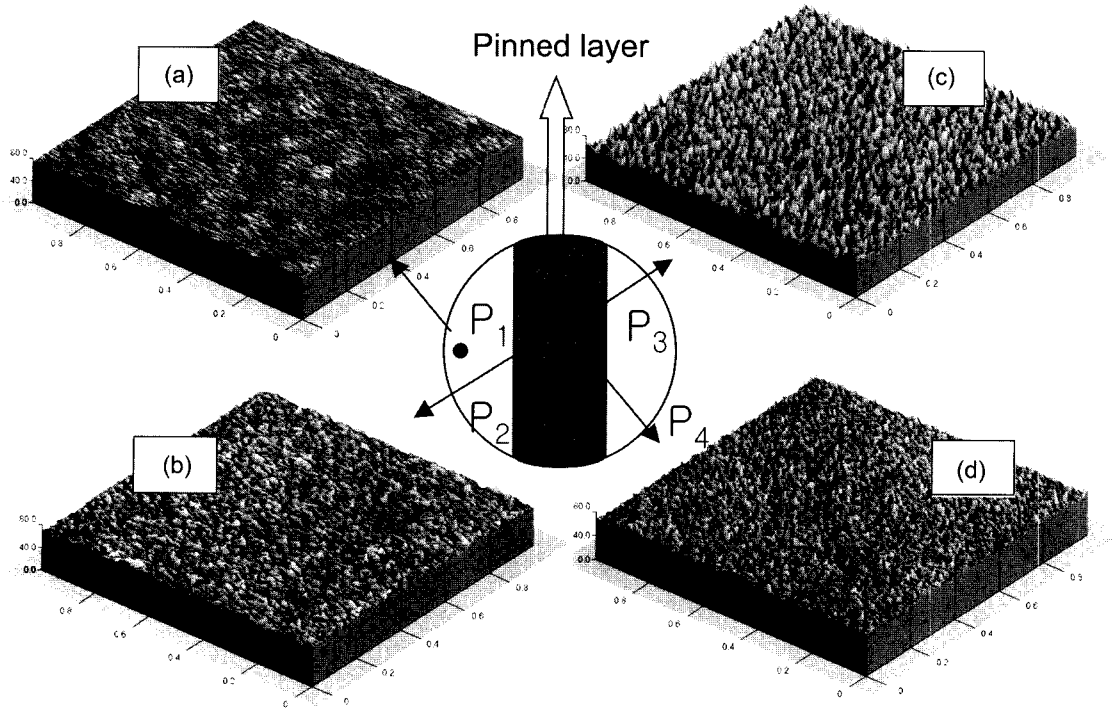

Fig. 7. AFM images across the pinned layer outside the junction, (a) at point p1, outside the layer, (b) point p2, near left edge, (c) point p3, center, and (d) point p4, near right edge. (scan area: 1×1 μm^2)

axes along the pinned layer. That is, the easy axis is governed by the annealing field direction while the saddle axis is always directed along the pinned-layer axis. These results indicate that the saddle shapes of H_c and H_{ua} are basically related to geometric effects during sample deposition.

3.2. Surface roughness

AFM images across the pinned layer outside the junction are shown in Figs. 7(a)~(d), at the measuring points p1-p4 depicted in the inset. At point p1, outside the layer, the root mean square (RMS) roughness is 1.4 Å, corresponding to the surface roughness of the Si substrate. Within the layer, the roughness increases to 2.5 Å at p2 near the edge, and 5.5 Å at p3 near the center of the layer, but then decreases to 2.7 Å near the left edge (p4).

Figures 8(a)~(d) are AFM images at several measuring points along the free layer across the junction. On the free layer outside the junction (point p5), RMS roughness is 3.3 Å, and becomes smaller, 2.3 Å, at the near edge (p6). The roughness increases to 5.7 Å as the measuring point moves to the center of the junction (p7), and then decreases as the point moves to the left edge (p8).

Figures 9(a) and (b) show the plot of RMS roughness versus measuring distance across the pinned layer, obtained from Figs. 7 and 8, respectively. The range of variation of RMS roughness is nearly the same, from 2.5 Å to 5.8 Å, and reveals symmetric variation with respect to the center of the pinned-layer axis. However, the variation near the edge is greater when roughness is measured on the free layer across the junction. Here, it is noted that the flatness at the edge point (p6) is better than that on the free-layer region (p5). These variations are quite similar to those of film thickness, as shown in the inset figures. This may be a geometric effect of the deposition process using a shadow mask, but it is hard to understand its mechanism in detail.

In Figs. 5(b) and 6(b), the H_{ua} distribution shape represents the amount of coupling between layers. The H_{ua} (~20 Oe) at the junction center is about 4 times that near the edge (~5 Oe). There is an insulating Al_2O_3 layer between the free and pinned (and antiferromagnetic) layers. Thus, Neel's orange peel coupling by dipole interaction could be dominant over RKKY-like interaction. The exchange coupling H_N is generally expressed as [10]:

$$H_N = \frac{\pi^2 h^2}{\sqrt{2} t_F \lambda} M_p \exp(-2\pi\sqrt{2} t_s/\lambda) \quad (1)$$

where h and λ are the height and wavelength of the sinusoidal roughness respectively, t_F and t_S are the thickness of the free layer and the distance between two

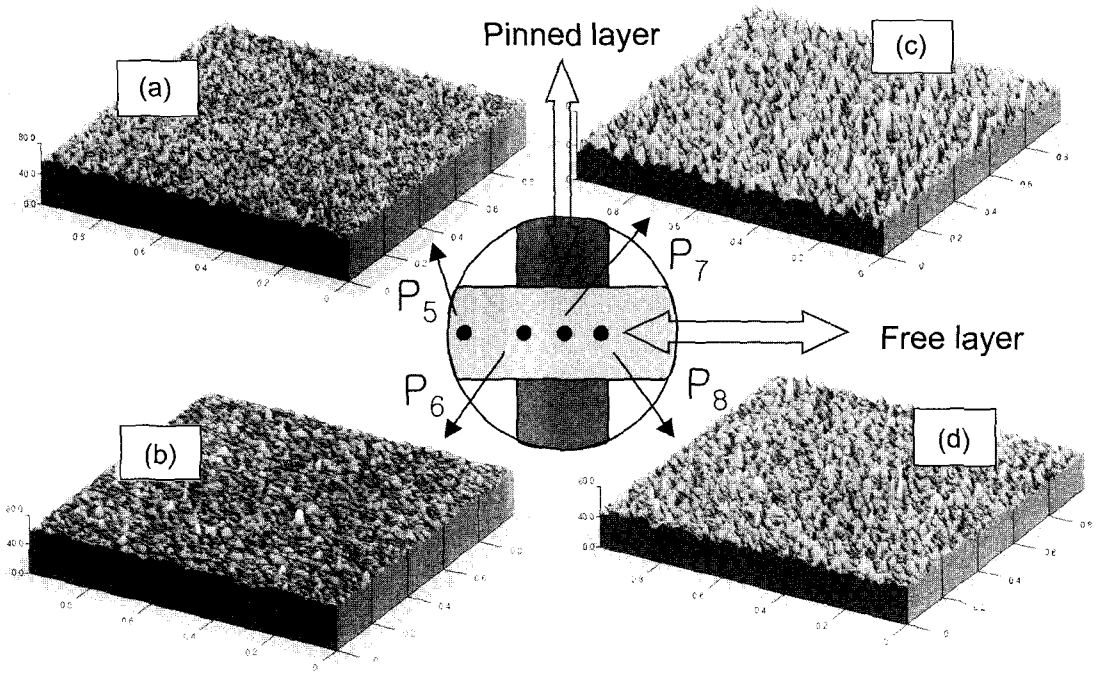

Fig. 8. AFM images along the free layer across the junction, (a) at point p5, outside the layer, (b) point p6, near left edge, (c) point p7, junction center, and (d) point p8, near right edge. (scan area: 1×1 μm^2)

layers respectively, and M_p is the saturation magnetization of the pinned layer.

The M_p could be constant irregardless of pined layer thickness. When thickness t_F is taken into account in denominator, the small increase of at both edges of junction along pinned layer, in Figs. 5(b) and 6(b), is described by the decreasing t_F at edges. But along free layer could be decreased inside the junction area, opposite tendency to measured one along pinned layer. Because the exchange coupling is given as a square function of roughness height h, the coupling at the junction center along free layer is expected to be 4-5 times that near the edge from the roughness shown in Fig. 9. There is good agreement between the measured and expected H_{ua} variations, suggesting that H_{ua} in the free layer is well described by dipole interaction between the free and pinned layers.

3.3. Annealing field effect

The variations of H_c and H_{ua} are compared in Figs. 10(a)~(c) for annealing field angles $\theta_a = 0$, 45°, and 90°, respectively. Here, the loops are measured in a field along the annealing field direction, and the legends of x-axis mean the distance along the measured directions. For the 45° annealed sample, both H_c and H_{ua} have a relative plateau regime over the junction area, compared to the $\theta = 0°$, 90° samples. It is not easy to evaluate the annealing field effect clearly, but topological distribution of magnetization reversals could discriminate its effect.

The reversal field H_r for increasing fields is approximated by the sum of H_c and H_{ua}, and the reversal field H_r for decreasing fields is the difference between H_c and H_{ua}, i.e., H_{ua}-H_c [15]. The sum of H_c and H_{ua} could reflect the distribution of reversal field in an increasing field. Thus, the topological distribution of the reversal field is obtained by sorting the sum of H_c and H_{ua}.

Figure 11 shows the distribution of the sum of H_c and H_{ua}, that is, the topological distribution of the reversal field, where the lines represent Gaussian fitting curves for corresponding data. The field for maximum counter number are 40 Oe, 35 Oe, and 35 Oe for annealing field angles $\theta_a = 0°$, 45°, and 90°, respectively. However, the field regime for full width at half maximum on the θ_a = 45° sample is relatively small, at about 8 Oe. This suggests that there is some effect of the annealing field angle on reversal magnetization, and that its distribution is relatively narrow for the 45° sample, compared to the θ_a = 0° and 90° samples.

3.4. Average of local distribution

When the beam size is expanded over the entire junction area, the measured M-H loop should reflect the average of the local distribution. Figure 12 shows the M-H loop for expanded beam size over the junction area on an annealed sample with $\theta_a = 0°$. Here, two loops are superimposed: one loop without shift corresponds to the

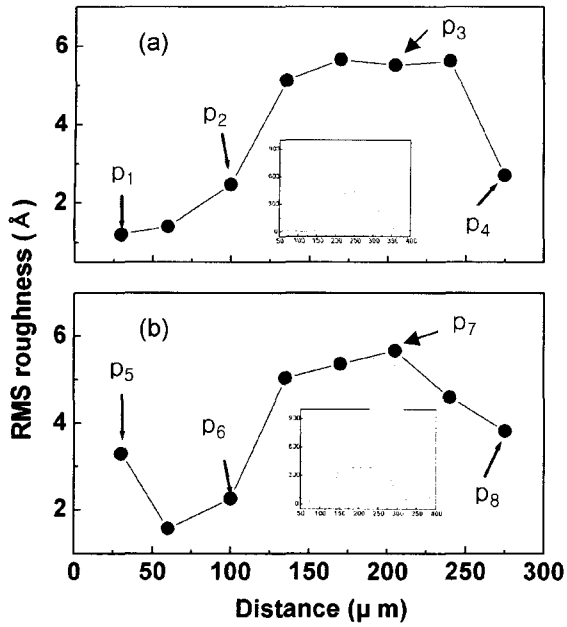

Fig. 9. Variation of average surface roughness (a) across the pinned layer outside junction and (b) inside junction.

area outside the junction along the free-layer axis, and another loop with shift corresponds to the area inside the junction. Even in the loop for the junction, the field regime for magnetization reversal is wide; that is, the magnetization reversal starts from 35 Oe and ends at 45 Oe. This regime of reversal distribution is in agreement with the value obtained from the topological distribution in Fig. 11(a). This agreement suggests that magnetization is not uniform over an entire junction area, and that macroscopic properties are governed by the averages of their local distributions.

4. Conclusion

Local M-H loops have been measured on the free-layer of TMR junctions using a MOKE system, where the optical beam size is about 2 μm diameter. Tunnel junctions were deposited using a DC magnetron sputtering method in a chamber having a base pressure of 3×10^{-9} Torr. There is a gradual increase of magnetization as the measuring point moves inwards from the edge, due to the gradual change of film thickness. Irregular variations are revealed in as-deposited samples even near the center, but the magnetization is smoothed out over the junction area after annealing.

Relatively irregular variations of coercive force H_c (~17.5 Oe) and unidirectional anisotropy field H_{ua} (~7.5 Oe) in as-deposited samples are revealed. After annealing at 200 °C, H_c decreases to 15 Oe, but H_{ua} increases to 20

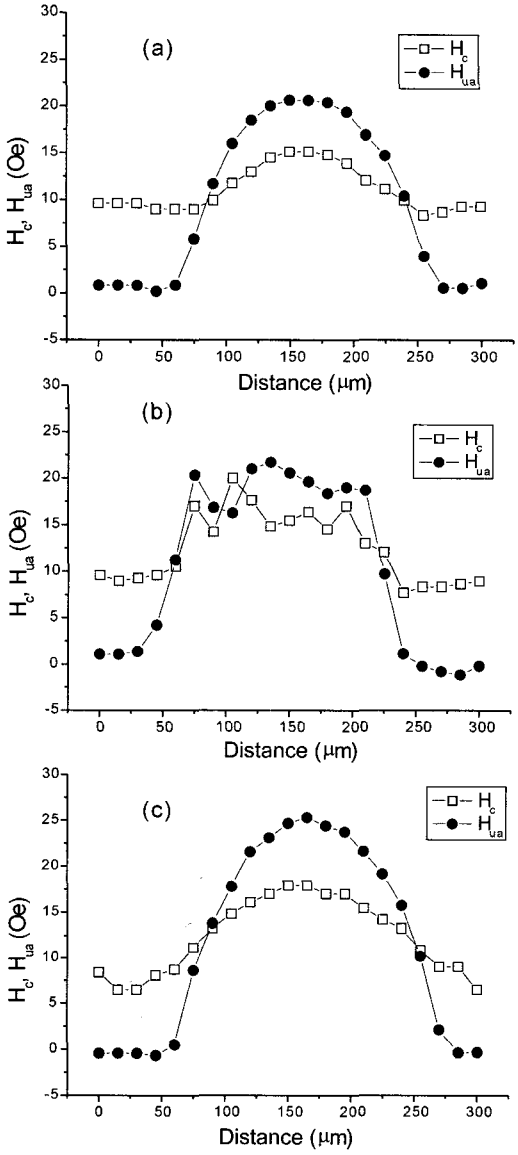

Fig. 10. Variations of H_c and H_{ua} in 200 °C-annealed sample for angles $\theta_a = 0°$, 45°, and 90°, respectively. The legend of x-axis means the distance along the measured directions.

Oe with smooth local variations. Two-dimensional plots of H_c and H_{ua} show symmetric saddle shapes with their axes on the pinned layer, irrespective of the annealing field angle, due to the geometric effect during deposition together with a minor annealing effect. In addition, the variation of RMS surface roughness is revealed to be symmetric with respect to the center of the pinned-layer axis, 2.5 Å near the edge and 5.8 Å at the junction center.

H_{ua} could be uniform over the junction area when thickness is taken into account in dipole interactions. However, roughness is involved in dipole interactions, so the coupling at the junction center is expected to be 4-5 times that at the near edge. There is good agreement

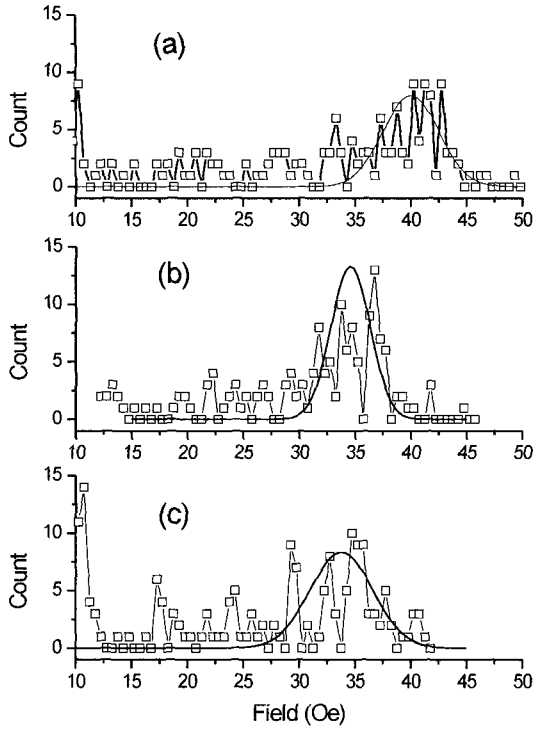

Fig. 11. Topological distribution of reversal field $H_r=H_c+H_{ua}$, for angles $\theta_a = 0°$, 45°, and 90°, respectively, where the lines represent Gaussian fitting curves for corresponding data.

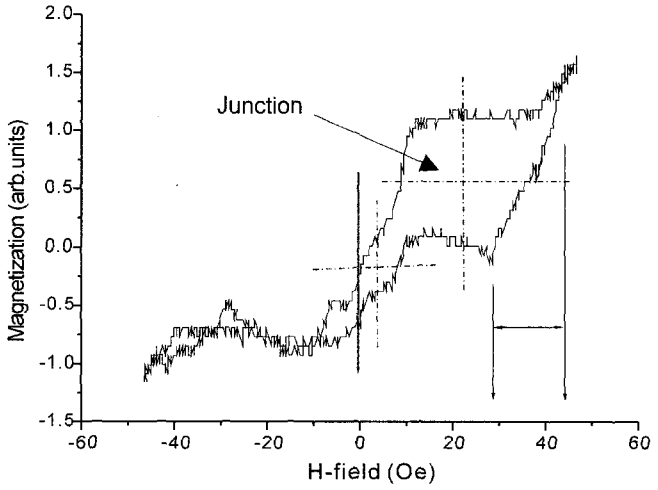

Fig. 12. M-H loop for expanded light beam over entire junction area in 200 °C-annealed sample for the annealing field angle $\theta_a = 0°$. (Two loops are superimposed; one corresponding to the free layer outside the junction, and the other to the junction.)

between the measured and expected H_{ua} variations, suggesting that H_{ua} of the free layer is well described by dipole interaction between the free and pinned layers, and/or the antiferromagnetic MnIr layer. As a whole, the reversal magnetization is not uniform over the entire junction area and macroscopic properties are governed by the averages of the local distributions.

Acknowledgements

This work was supported by the Korean Science and Engineering Foundation through the Research Center for Advanced Magnetic Materials at Chungnam National University.

References

[1] S. S. S. Parkin, *et al.*, J. Appl. Phys. **85**, 5828 (1999).
[2] J. S. Moodera, L. R. Kinder, T. M. Wong, and R. Meservey, Phys. Rev. Lett. **74**, 3273 (1995).
[3] M. Julliere, Phys. Lett. **54A**, 225 (1975).
[4] J. C. Slonczewski, Phys. Rev. B. **39**, 6995 (1989).
[5] J. S. Moodera, L. R. Kinder, J. Nowak, P. LeClair, and R. Meservey, Appl. Phys. Lett. **69**, 708 (1996).
[6] L. Pust, L. E. Wenger, R. A. Lukaszew, Y. Sheng, D. Litvinov, Y. Wang, C. Uher, and R. Clarke, J. Appl. Phys. **85**, 5765 (1999).
[7] M. A. Ruderman, C. Kittel, Phys. Rev. **96**, 99 (1954).
[8] L. Neel, and C. R. Acad. Sci. Please check if this journal should be cited as Comp. Rendu Acad. Sci. **255**, 1676 (1962).
[9] C. Lee, J. A. Bain, S. Chu, and M. E. McHenry, J. Appl. Phys. **91**, 7113 (2002).
[10] J. C. S. Kools, W. Kula, D. Mauri, and T. Lin, J. Appl. Phys. **85**, 4466 (1999).
[11] S. Miura, M. Tsunoda, and M. Takahashi, J. Appl. Phys. **89**, 6308 (2001).
[12] J. X. Shen, and M. T. Kief, J. Appl. Phys. **79**, 5008 (1996).
[13] C. M. Park, K. I. Min, and K. H. Shin, IEEE Trans. **Magn-32**, 3422 (1996).
[14] C. Hou, J. Chen, M. T. Kief, Z. Gao, S. Mao, and T. Pokhil, Appl. Phys. Lett. **78**, 237 (2001).
[15] C. Hou, H. Fujiwara, and F. Ueda, J. Magn. Magn. Mater. **198-199**, 450 (1999).
[16] M. Tsunoda, K. Nishigawa, S. Ogata, and M. Takahashi, Appl. Phys. Lett. **80**, 3135 (2002).
[17] M. Tsunoda, and M. Takahashi, to be published in this volume, Korean J. Magnetics (2002).